JACS
JOURNAL OF THE AMERICAN CHEMICAL SOCIETY
Article
pubs.acs.org/JACS

Effect of Metal Ions on Photoluminescence, Charge Transport, Magnetic and Catalytic Properties of All-Inorganic Colloidal Nanocrystals and Nanocrystal Solids

Angshuman Nag,[†] Dae Sung Chung,[†] Dmitriy S. Dolzhnikov,[†] Nada M. Dimitrijevic,[‡,§] Soma Chattopadhyay,[⊥] Tomohiro Shibata,[⊥] and Dmitri V. Talapin*[,†,‡]

[†]Department of Chemistry and James Frank Institute, University of Chicago, Illinois 60637, United States
[‡]Center for Nanoscale Materials, [§]Chemical Sciences and Engineering, and [⊥]Advanced Photon Source, Argonne National Laboratory, Argonne, Illinois 60439, United States

Supporting Information

ABSTRACT: Colloidal semiconductor nanocrystals (NCs) provide convenient "building blocks" for solution-processed solar cells, light-emitting devices, photocatalytic systems, etc. The use of inorganic ligands for colloidal NCs dramatically improved inter-NC charge transport, enabling fast progress in NC-based devices. Typical inorganic ligands (e.g., $Sn_2S_6^{4-}$, S^{2-}) are represented by negatively charged ions that bind covalently to electrophilic metal surface sites. The binding of inorganic charged species to the NC surface provides electrostatic stabilization of NC colloids in polar solvents without introducing insulating barriers between NCs. In this work we show that cationic species needed for electrostatic balance of NC surface charges can also be employed for engineering almost every property of all-inorganic NCs and NC solids, including photoluminescence efficiency, electron mobility, doping, magnetic susceptibility, and electrocatalytic performance. We used a suite of experimental techniques to elucidate the impact of various metal ions on the characteristics of all-inorganic NCs and developed strategies for engineering and optimizing NC-based materials.

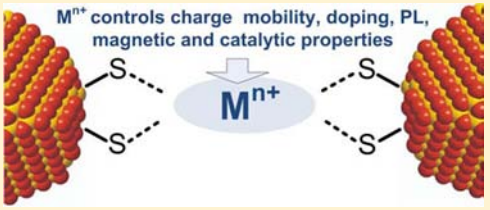

1. INTRODUCTION

Colloidal nanocrystals (NCs) represent a versatile class of materials with unique optical, electronic, magnetic, and catalytic properties. Semiconductor NCs with size dependent electronic structure provide exciting opportunities for solution-based fabrication of electronic and optoelectronic devices. They are actively explored as the building blocks for photovoltaics, thermoelectrics, light-emitting diodes, and photodetectors.[1−3] However, as-synthesized NCs are typically capped with insulating organic ligands that inhibit the injection or extraction of charge carriers from individual NCs. The most successful approach to enhance electronic coupling between NCs is to replace bulky and insulating organic ligands with small and electronically transparent inorganic ligands that result in all-inorganic colloidal NCs.[3,4] Typically, the surface of metal chalcogenide NCs exhibit numerous undercoordinated electrophilic metal sites that impair a strong affinity of NC surface toward nucleophilic inorganic ligands such as chalcogenides (S^{2-}, Se^{2-}, Te^{2-}), OH^-, NH_2^-, SCN^-, and Cl^- or molecular metal chalcogenide complexes (MCCs, e.g., $Sn_2S_6^{4-}$ and $In_2Se_4^{2-}$).[4−8] These anionic ligands (e.g., S^{2-}, $Sn_2S_6^{4-}$, etc.) covalently bind to the NC surface and form negatively charged Stern layer at the NC surface.[9,10] Electrostatic repulsion between charged NCs provides the colloidal stability in polar solvents. Alkali metal ions, NH_4^+, or $N_2H_5^+$ were typically used as the counterions for charge balance.[11] Because of their high solvation energy and low affinity toward the NC surface, these cations formed a diffuse layer around NCs. Recent research focused on designing the anionic part of inorganic ligands, while the role of cations remained largely unexplored. Previous works largely ignored the presence of counterions, typically by using thermally unstable cations (e.g., $N_2H_5^+$) that decomposed into gaseous species upon mild annealing. To the best of our knowledge, the only example where counterions imparted new properties to inorganically capped NCs was the use of didodecyldimethylammonium (DDA^+) ions for stabilization of MCC-capped NCs in nonpolar solvents to control self-assembly of long-range ordered NC superlattices.[12]

Recently there were numerous studies of cation exchange in semiconductor NCs.[13,14] For example, the small size of NCs dramatically facilitated ion diffusion, enabling fast and reversible cation exchange at room temperature,[13] in contrast to the poor reactivity of extended bulk solids, where ionic exchange requires high temperature and/or pressure.[15] For example, the addition of Ag^+ ions in methanol to a colloidal solution of CdSe NCs resulted in the formation of Ag_2Se NCs due to lower free energy of silver chalcogenide phase and due to preferential solvation of Cd^{2+} ions by methanol.[13] In some cases such ion exchange is very fast and efficient, whereas in many other cases the addition of foreign ions to NC lattice has proven to be very difficult because of self-purification.[16,17] This

Received: February 8, 2012
Published: July 20, 2012

   dx.doi.org/10.1021/ja301285x | J. Am. Chem. Soc. 2012, 134, 13604−13615

work focuses on the systems following the second scenario. In all experiments we modified the ligands chemically bound to the NC surface while the composition of parent NCs remained unaltered.

In this work we used the cationic part of inorganic ligands to systematically engineer the NC properties and to impart additional functionalities to all-inorganic NCs. We found that cations provide a very convenient tool for tailoring optical, electronic, magnetic, and catalytic properties of all-inorganic NCs and NC solids. We show that Cd^{2+}, Ca^{2+}, or In^{3+} can bind to the NC surface in solution and inverse the surface charge from negative to positive, along with dramatic improvement of luminescence efficiency. In a NC film, cations can link adjacent NCs and improve electron mobility; cations (e.g., K^+, In^{3+}) can switch conductivity in CdTe NC solids from p-type to ambipolar to n-type. Mn^{2+} can bridge S^{2-}-capped CdSe NCs via S−Mn−S bonds and impart magnetic properties to originally diamagnetic CdSe NCs. Finally, bridging semiconductor NCs with Pt^{2+} ions offers control over electrocatalytic properties of NC solids.

2. EXPERIMENTAL SECTION

2.1. Nanocrystal Synthesis. First, 4.4 nm zinc blende CdSe NCs capped with oleic acid were prepared following Cao et al.,[18] and 4.2 nm wurtzite CdSe NCs capped with octadecylphosphonic acid were prepared from CdO and *n*-trioctylphosphine selenide following Manna et al.[19] Zinc blende and wurtzite NCs showed similar results in all studies discussed in this article. We also used CdSe/ZnS core/shell NCs capped with proprietary amine-based ligands obtained from Evident Technologies Inc. (Troy, NY). InAs NCs capped with trioctylphosphine were prepared by reacting $InCl_3$ and $As[Si(CH_3)_3]_3$.[20,21] CdS nanorods were prepared via a slightly modification of the procedure described in ref 22. CdTe NCs capped with tetradecylphosphonic acid (TDPA) were prepared following ref 23 with minor modifications.

2.2. Ligand Exchange. The exchange of original organic ligands with S^{2-} and Te^{2-} was carried out following our previous works.[4,6] In a typical experiment, 1 mL (5 mg/mL) of organics-capped CdSe NCs dispersion in toluene was combined with 1 mL of K_2S solution (12 mg/mL) in formamide (FA) and stirred for about 10 min, leading to a complete phase transfer of NCs from toluene to the FA phase. The FA phase was separated out and washed three times with toluene. NCs were then precipitated by adding a minimum amount (∼0.8 mL) of acetonitrile, centrifuged, and re-dispersed in FA. A similar ligand exchange with $Na_2Sn_2S_6$ was carried out following ref 24. All ligand exchange reactions were carried out in a glovebox filled with dry nitrogen.

2.3. NC Charge Inversion and Photoluminescence (PL) in solution. For studies of charge inversion and PL efficiency, 1 mL of a dilute solution (0.3 mg/mL) of K_2S-capped CdSe or CdSe/ZnS NCs in FA was combined with 2 mL of a FA solution of a salt containing desired cation and an anion with low nucleophilicity ($NaNO_3$, KNO_3, $Zn(NO_3)_2$, $Ca(NO_3)_2$, $Mg(NO_3)_2$, $Cd(NO_3)_2$ or $Cd(ClO_4)_2$, $Ba(NO_3)_2$, $In(NO_3)_3$, $Al(NO_3)_3$, etc.). Most of the data presented in this work correspond to 5 mM solutions of different cations. To ensure colloidal stability, all NC solutions were filtered through 0.2 μm PTFE syringe filter prior to optical measurements. The NC solutions retained their colloidal stability in the presence of some metal ions for several days. To eliminate variations, we always used freshly prepared mixtures of NCs and metal ions for all optical and zeta-potential measurements. The solutions were typically handled inside a N_2-filled glovebox.

2.4. Linking NCs with Inorganic Cations and Fabrication of Field-Effect Transistor (FET) Devices. First, ∼20 nm thick films of inorganically capped NCs were prepared by spin-coating (2000 rpm, 60 s) solutions of K_2S-capped CdSe NCs (∼20 mg/mL) in FA on a suitable substrate at an elevated temperature (80 °C) using an infrared lamp placed above spin-coater. Quartz substrates were used for UV−visible measurements, and heavily p-doped Si wafers (Silicon Quest, Inc.) with a 100 nm thick layer of thermally grown SiO_2 gate oxide were used for FET measurements. Substrates were hydrophilized by oxygen plasma or piranha (H_2SO_4:H_2O_2) treatments. Dried NC films were dipped into 50 mM solutions of metal salts ($Cd(NO_3)_2$, $Zn(NO_3)_2$, $In(NO_3)_3$, and $Mn(NO_3)_2$) in methanol for 30 min, followed by washing the films in pure anhydrous methanol. For FET measurements, the cation-treated NC films were annealed at 200 °C for 30 min to remove solvents and any volatile species without sintering the NCs. The NC film thickness was measured using AFM. The aluminum top source and drain electrodes were thermally evaporated at 1−2 Å/s rate up to ∼1000 Å total thickness using a metal evaporator installed inside a glovebox. The FET channel length was 150 μm for devices with bottom gate and top source−drain electrodes. After deposition of top electrodes, the devices were annealed at 80 °C for 30 min to improve the contacts. All steps were carried out under N_2 atmosphere inside a glovebox. For the CdTe NC devices, we used both bottom gate/top source−drain FET geometry (channel length 150 μm) and bottom gate/bottom source−drain FET geometry (channel length 5 μm) with Au or Al source and drain electrodes.

Electrical measurements were carried out under quasi-static conditions with slow scan of source−drain or source−gate voltage using Agilent B1500A semiconductor parameter analyzer and homemade probe station placed inside a N_2-filled glovebox. The transfer characteristics for the FETs were measured with the gate voltage (V_G) sweep rate of 40 mV/s. The linear regime mobility (μ_{lin}) and the saturation regime mobility (μ_{sat}) were calculated from FET transfer characteristics as described in the Supporting Information.[25]

2.5. Characterization. Continuous-wave EPR experiments were carried out using a Bruker ELEXSYS E580 spectrometer operating in the X-band (9.4 GHz) mode and equipped with an Oxford CF935 helium flow cryostat with an ITC-5025 temperature controller. Magnetic properties were studied using SQUID magnetometry (MPMS XL, Quantum Design). Zero-field-cooled (ZFC) and field-cooled (FC) studies were recorded in the 5−300K range at H = 100 Oe after cooling the NC samples in zero field or in a 100 Oe field, respectively. Mn K-edge EXAFS measurements were carried out at the MRCAT 10-ID beamline at the Advanced Photon Source, Argonne National Laboratory, in the fluorescence mode with ionization chamber in Stern−Heald geometry for the NC samples. Samples were loaded in a Teflon sample holder inside a N_2-filled glovebox and sealed inside an airtight chamber. Mn standard samples were measured in the transmission mode. The sulfur K-edge XANES spectra were measured at 9-BM beamline at the Advanced Photon Source in the fluorescence mode. The EXAFS data were processed using Athena software[26] by extracting the EXAFS oscillations $\chi(k)$ as a function of photoelectron wavenumber k following standard procedures. The theoretical paths were generated using FEFF6,[27] and the models were fitted using Artemis software.[28] The Artemis package was also employed to refine the fitting parameters used for modeling each sample in the *R*-space until a satisfactory model describing the system was obtained. For EPR, magnetic, and EXAFS/XANES measurements, samples were prepared in the form of thoroughly washed and dried powders of CdSe/S^{2-} NCs cross-linked with Mn^{2+} ions.[25]

Electrochemical measurements were carried using a Gamry Reference 600 potentiostat with a three-electrode electrochemical cell. For electrochemical measurements in anhydrous acetonitrile, we used 0.1 M tetrabutylammonium perchlorate (TBAP) as the electrolyte. Glassy carbon (GC), platinum wire, and Ag/Ag^+ (0.01 M $AgNO_3$ in CH_3CN) were used as the working, counter, and reference electrodes, respectively. The area of GC electrode was 7.07×10^{-2} cm^2. The NC films were formed at the surface of a GC electrode by drop-casting. For optical studies, ITO-covered glass was used as the working electrode with a NC film prepared by spin-coating. As a proton source for electrochemical measurements in acetonitrile, we used dimethylformamide (DMF) protonated by trifluoromethanesulfonic (triflic) acid. Protonated DMF was synthesized using a slight modification of the method described in ref 29. In

brief, equimolar amounts of triflic acid and DMF were mixed and stirred for 2−3 min, resulting in the formation of a white solid soluble in acetonitrile and dichloromethane. Typical $[H(DMF)]^+OTf^-$ concentration used in this work was 0.01 M.

For electrochemical measurements in aqueous solutions, pH was buffered at 6.50 by a phosphate buffer (a mixture of K_2HPO_4 and KH_2PO_4 with total concentration of phosphate 0.15 mol/L). GC, platinum wire, and Ag/AgCl/(saturated KCl solution) were used as the working, counter, and reference electrodes, respectively. The area of the GC electrode was 7.07×10^{-2} cm^2. The NC films were prepared at the surface of GC by drop-casting. All solutions were carefully degassed and kept under a nitrogen atmosphere.

3. RESULTS AND DISCUSSION

3.1. Charge Inversion of Inorganically Capped Nanocrystals. First, 4.2 nm CdSe NCs were transferred from toluene into a polar solvent (FA) by treatment with K_2S that exchanged original *n*-tetradecylphosphonate surface ligands with S^{2-} as described in ref 30. The degree of ligands exchange has been confirmed by FTIR measurements showing complete removal of the absorption bands around 3000 cm^{-1} corresponding to C−H stretching in the hydrocarbon tails of the organic ligands (Figure S1). In agreement with our previous studies, S^{2-} covalently bonded to the NC surface (Figure 1A), resulting in negatively charged CdSe NCs with measured electrophoretic mobility of -0.7×10^{-8} m^2 V^{-1} s^{-1} and ζ-potential of −35 mV calculated using Henry's equation.[31] By knowing the ionic strength, we can also calculate surface charge density (σ).[25] For a spherical particle immersed in an electrolyte, $\sigma = \varepsilon_0\varepsilon\zeta(1 + \kappa r)/r$, where ε_0 is the vacuum permittivity, ε (109 for FA) is the dielectric constant of solvent, r is the hydrodynamic radius of NC, and k^{-1} is the Debye screening length in electrolyte.[12,32] The average surface charge of a spherical NC, Z, in units of elementary charges (e) can be obtained as $Z = 4\pi r^2\sigma/e$. For K_2S-capped 4.2 nm CdSe NCs (CdSe/S^{2-} NCs, $\zeta = -35$ mV) we obtained $\sigma = -0.016$ C/m^2, or ∼9 negative elemental charges accumulated at the surface of CdSe NCs (calculation details provided in Supporting Information). These numbers should be viewed as conservative estimates because ζ-potential defines the electrostatic potential not exactly at the NC surface but at the slipping plane that separates mobile solvent from the solvent coordinated to the NC surface. In addition, any not accounted residual electrolyte would result in underestimation of the NC charge.

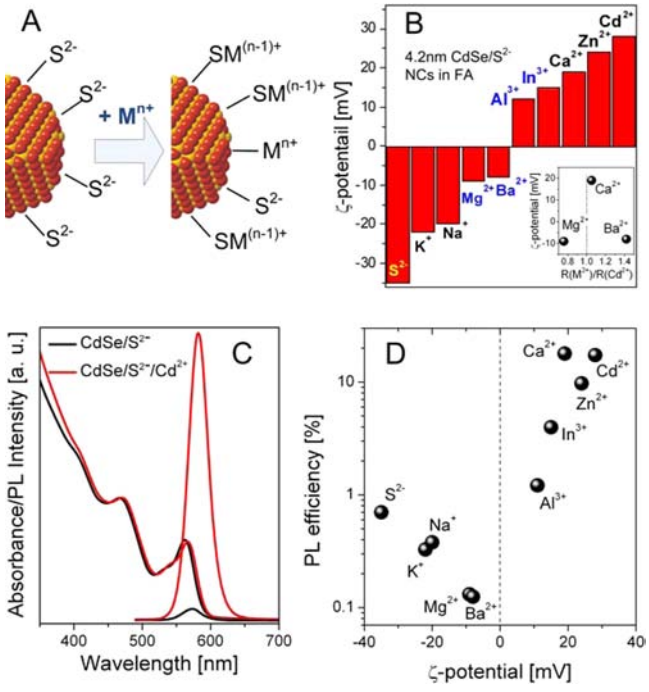

Figure 1. (A) Schematic representation of surface charges for K_2S-capped CdSe NCs, before (left) and after (right) treatment with strongly binding metal ions M^{n+}. (B) Variations of ζ-potential of K_2S-capped CdSe NCs in formamide in the presence of 5 mM various metal ions. The inset shows the variation of ζ-potential in the Mg^{2+}, Ca^{2+}, Ba^{2+} series plotted against the metal ion radius relative to the ionic radius of Cd^{2+}. (C) UV−vis absorption and PL spectra of CdSe NCs capped with K_2S, before and after addition of 5 mM Cd^{2+} ions. (D) Room-temperature PL efficiency of CdSe/S^{2-} NCs in the presence of different metal ions, plotted against ζ-potential.

Negatively charged chalcogenide ions bound to CdSe NC surface should interact electrostatically with nearby cations. In addition, they may exhibit specific chemical affinity toward metal ions that form strong chemical bonds with chalcogens (Figure 1A). In a polar solvent, these interactions can be monitored by measuring changes of electrophoteric mobility in the presence of specific cations. We found that addition of 5 mM of various metal salts to a dilute (0.3 mg/mL) solution of CdSe/S^{2-} NCs resulted in significant changes of ζ-potential. Since ζ-potential and amount of surface cation vary with NC size, all the quantitative comparisons were carried out for NCs with the same size. Figure 1B shows that the ζ-potential of 4.2 nm CdSe NCs in FA can be tuned almost continuously from −35 mV for CdSe/S^{2-} to +28 mV for CdSe/S^{2-}/Cd^{2+}, depending upon the chemical nature of added cation. Figure 1B shows data for ζ-potentials in the presence of 5 mM of different metal ions. In Figure S2 we adjusted the concentrations of each $M(NO_3)_n$ salt to the total ionic strength of 15 mM (corresponding to 5 mM concentration of divalent metal nitrate, $n = 2$), revealing the same trend of ζ-potentials. When K^+ or Na^+ was added to the NC solutions in the form of nitrates, the absolute value of ζ-potential decreased from −35 to about −20 mV which could be explained by the increase of the ionic strength without specific binding of metal to NC surface. This scenario agrees with the Derjaguin−Landau−Verwey−Overbeek (DLVO) theory[9,10,33] that takes into account Coulombic interactions of colloidal particles with point-like charges. However, the DLVO theory cannot explain the interaction of CdSe NCs with other cations, such as Al^{3+}, In^{3+}, Zn^{2+}, Ca^{2+}, and Cd^{2+} that resulted in the charge inversion as shown in Figure 1B. For example, the addition of 5 mM Cd^{2+} in the form of $Cd(NO_3)_2$ or $Cd(ClO_4)_2$ to 0.3 mg/mL solution of 4.2 nm CdSe/S^{2-} NCs in FA yielded +28 mV ζ-potential. This corresponds to ∼11 elemental charges (σ = +0.018 C/m^2) associated with CdSe/S^{2-} NCs exposed to 5 mM Cd^{2+} solution.[25] After addition of Mg^{2+}, Ba^{2+}, Al^{3+}, or In^{3+} to CdSe/S^{2-} NCs, the magnitude of ζ-potential was less than 15 mV, resulting in a limited colloidal stability (Figure 1B, blue symbols) and causing difficulties for accurate quantitative estimation of ζ-potentials. Charge inversion has been also observed in the case of CdSe NCs capped with MCC ligands such as $Sn_2S_6^{4-}$ (Figure S3). The reproducibility of reported trends has been verified in multiple control experiments. At this point we can only speculate about detailed bonding motifs between NCs and metal ions. These should depend on the chemical nature of NCs and metal ions; some possibilities are shown in Figure 1A. Additional structural studies will be provided in section 3.6.

dx.doi.org/10.1021/ja301285x | J. Am. Chem. Soc. 2012, 134, 13604−13615

The charge inversion, where interfacial charges attract counterions in excess of their own nominal charge, has been previously seen in lipid vesicles, in latex colloids, and at the mercury/water interface[9,10,33] In general, charge inversion does not require a specific binding of opposite charges. It can result from the effect of correlation between multiple charged ions near the interface, not accounted by the mean-field theories such as DLVO.[9] For example, Shklovskii has shown that screening of a strongly charged particle by multivalent counterions can generate an inverted charge Q^* with magnitude up to $Q^* \approx 0.83(QZe)^{1/2}$, where Q is the original particle charge and Ze is the charge of the counterions.[34] This theory, also confirmed by numerical simulations,[35] predicts for 4.2 nm CdSe NCs with $Q = -9e$ a maximum inverted charge of $Q^* = 3.5e$ in the presence of divalent cations. This predicted Q^* is significantly smaller than the inverted charge ($Q^* = 11e$) calculated from the measured electrophoretic mobility of $CdSe/S^{2-}/Cd^{2+}$ NCs in the presence of 5 mM Cd^{2+} ions. In addition, Figure 1B shows that highly charged cations (Al^{3+}, In^{3+}) generate smaller charge inversion than Ca^{2+}, Zn^{2+}, and Cd^{2+}. Moreover, the addition of Ca^{2+} ions results in a strong charge inversion, whereas Mg^{2+} and Ba^{2+} with similar charge and chemical properties do not show this effect at all (Figure 1B, inset). These observations suggest that charge inversion of $CdSe/S^{2-}$ NCs cannot be explained by the electrostatic mechanism and requires analysis of chemical interactions between NCs and metal ions. Indeed, the addition of Cd^{2+} ions to CdSe NCs results in a small but reproducible (~4 nm or ~16 meV) red-shift of the excitonic peaks in UV–vis and PL spectra (Figure 1C), consistent with a small increase in the effective NC diameter due to surface binding of Cd^{2+}. Other metal ions resulted in even smaller shifts of the absorption maximum, ruling out possible cation exchange reactions inside the NCs (Figure S4). However, one needs to be careful because certain metal ions at a sufficiently high concentration can initiate cation exchange reactions inside the NCs.[13]

The charge inversion should be facilitated by high affinity of the counterion to NC surface and by lower solvation energy of the counterion.[9,10,13] In our case, there are indications that softer cations have higher affinity ($Cd^{2+} > Zn^{2+}$; $In^{3+} > Al^{3+}$) to $CdSe/S^{2-}$ NC surface, exposing soft basic sites like $S^{\delta-}$ and $Se^{\delta-}$.[36] Generally, cation hardness and solvation energy in polar solvents decrease down the group in the periodic table; thus, the charge inversion efficiency for $CdSe/S^{2-}$ NC is expected to follow the trend $Mg^{2+} < Ca^{2+} < Ba^{2+}$. However, in this list of chemically similar cations, only Ca^{2+} induced charge inversion, whereas addition of Mg^{2+} and Ba^{2+} resulted in the aggregation of NCs (Figure 1B). It is difficult to fully rationalize this trend; however, a comparison of ionic radii of metal ions to the radius of Cd^{2+} ions shown in the inset to Figure 1B provides a preliminary suggestion. One can see that Mg^{2+} ions are too small and Ba^{2+} ions are too large to match the lattice constant at the surface of CdSe NCs, while the ionic radius of Ca^{2+} is only about 5% larger than that of Cd^{2+}, offering an excellent match to the CdSe lattice. Due to the similarity in ionic radii, we may expect the formation of an epitaxial adlayer of CaS at the surface of CdSe NCs. It is difficult to completely rule out minor incorporation of Ca^{2+} into CdSe lattice via displacement of Cd^{2+} ions. At the same time, Ca^{2+} and Cd^{2+} are isovalent, and such exchange should not result in any significant changes of ζ-potential. The trends for ζ-potential shown in Figure 1B,D require specific binding of charged ions to the NC surface. The effect of ionic size on specific adsorption was previously observed for various crystal surfaces.[37] Thus, in addition to chemical affinity, ionic radii can play an important role in the interaction of metal ions with surface of all-inorganic NCs.

3.2. Correlation between Charge Inversion and PL Efficiency. We revealed a clear correlation between ζ-potential and PL efficiency, as shown in Figure 1D. The metal ions providing large charge inversion also resulted in a large increase of PL efficiency. For example, we observed a 25-fold increase of PL efficiency from 0.7% for $CdSe/S^{2-}$ to 17.3% upon addition of 5 mM Cd^{2+} ions. The PL efficiency is a very sensitive probe of the NC surface. Such correlation between surface charge and PL efficiency makes sense because previous studies have shown that CdSe NCs with metal-rich surface exhibited higher PL efficiency due to reduced concentration of surface traps.[38] In our case, the increase of PL efficiency can also be explained by binding metal ions to the surface of $CdSe/S^{2-}$ NCs. At the same time, we observed some counterintuitive trends that deviate from the current understanding of surface passivation for CdSe NCs. First, we found that Cd^{2+} and Ca^{2+} ions provided higher PL efficiency than Zn^{2+}, despite the fact that ZnS is known as an excellent material to passivate surface of CdSe NCs confining both electron and hole in the core.[39,40] Even more intriguing, the same trend was observed when we added metal ions to $CdSe/ZnS/S^{2-}$ NCs: the addition of Cd^{2+} and Ca^{2+} ions reproducibly yielded higher PL efficiency than Zn^{2+} (Figures 2A and S5). This trend was observed for several batches of CdSe/ZnS core–shells synthesized in-house or obtained from different commercial sources. The addition of Cd^{2+} or Ca^{2+} increased PL efficiency to nearly 60% that was close to the efficiency of original, organically capped NCs. One possible explanation could be that Zn^{2+} ions are better solvated by FA molecules compared to Cd^{2+} and Ca^{2+} and therefore exhibit weaker affinity to the surface of CdSe or CdSe/ZnS NCs. This study also points to potential utility of calcium salts as shell materials for luminescent NCs. To the best of our knowledge, this possibility has not been explored before. It should be noted that Ca^{2+} typically forms solids with octahedrally coordinated Ca^{2+} sites instead of tetrahedrally coordinated Cd^{2+} sites in CdSe lattice. It could therefore be used as a shell material for lead chalcogenide NCs.

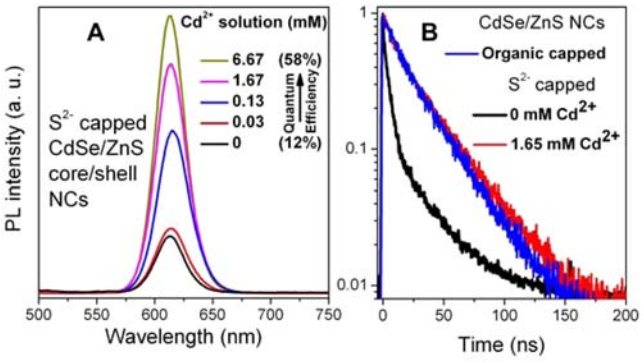

Figure 2. (A) Photoluminescence spectra for CdSe/ZnS NCs capped with K_2S in the presence of different concentrations of Cd^{2+} ions. (B) PL decay profiles for CdSe/ZnS NCs with different surface modifications. The excitation wavelength was 400 nm.

Time-resolved PL decay studies for CdSe/ZnS NCs before and after treatment with Cd^{2+} ions suggest that observed PL increase resulted from the suppression of non-radiative recombination channels introduced by S^{2-} ligands (Figure

dx.doi.org/10.1021/ja301285x | J. Am. Chem. Soc. 2012, 134, 13604–13615

2B). In presence of 5 mM Cd^{2+} ions, the PL decay of CdSe/ZnS NCs closely matched that of the original organics-capped NCs (Figure 2B). In addition to chemical passivation of surface dangling bonds, positively charged ions adsorbed at the NC surface can generate an electric field pushing holes away from the NC surface. Improved surface passivation for individual all-inorganic NCs also suggests the use of cations for engineering physical and chemical properties of NC solids.

3.3. Cation Bridges Determine Electron Mobility in All-Inorganic Nanocrystal Arrays. In the previous subsection we showed that metal ions, such as Cd^{2+}, can bind directly to the surface of CdSe/S^{2-} NCs, resulting in a charge inversion in dilute (~0.1−0.3 mg/mL) colloidal solutions. However, when the concentrations of CdSe/S^{2-} NCs and Cd^{2+} ions were increased to 10 mg/mL and 50 mM, respectively, we observed immediate precipitation of CdSe NCs (Figure S6). At the same time, the addition of 0.15 M $NaNO_3$ with ionic strength identical to the ionic strength of 0.05 M $Cd(NO_3)_2$ did not cause precipitation of CdSe/S^{2-} NCs (Figure S6), ruling out the ionic strength as the sole cause of colloidal instability. We therefore concluded that precipitation of NCs was a result of linking CdSe/S^{2-} NCs with Cd^{2+} ions, as shown schematically in Figure 3B. The elemental analysis of precipitated CdSe/S^{2-}/Cd^{2+} NCs revealed no original K^+ counterions, suggesting that Cd^{2+} completely displaced K^+ during aggregation of NCs. No K^+ ions were detected in the XPS spectra of precipitated NC solids. We then applied this treatment to the close-packed films of CdSe/S^{2-} NCs, originally charge-balanced with K^+ ions.

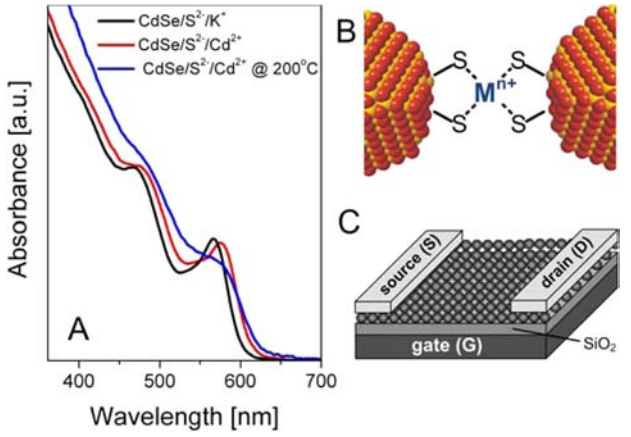

Figure 3. (A) UV−vis absorption spectra for a film of CdSe NCs capped with K_2S before and after treatment with Cd^{2+} ions. The measurements were carried out using an integrating sphere. (B) Schematics of NC linking with metal ions. (C) Schematics of a field-effect transistor used for studies of electronic coupling in the NC solids.

Transmission electron microscopy of all-inorganic NC solids revealed no changes in NC size and shape associated with the exchange of original organic ligands with S^{2-} ions (Figure S7). When K^+ was used as the counterion, we observed ~1 nm separations between adjacent NCs on a TEM grid, which could be a result of the electrostatic repulsion between negatively charged NC surfaces. On the other hand, the same NC solids treated with Cd^{2+} or In^{3+} ions nearly touched each other (Figure S7), suggesting the presence of an additional force pulling the NCs together. The absorption spectra of CdSe/S^{2-} NC films red-shifted by ~10 nm (38 meV) and broadened after dipping into a 50 mM solution of $Cd(NO_3)_2$ in methanol, suggesting enhanced electronic coupling between the NCs (Figure 3A). To gain a better insight into the electronic coupling, we measured charge carrier mobility in the arrays of CdSe/S^{2-} NCs bridged with different cations. For these studies we fabricated bottom-gated thin-film FETs with top source and drain electrodes (Figure 3C). The films (~20 nm thick) of K_2S-capped CdSe NCs were deposited by spin-coating on highly doped Si wafers with 100 nm thick SiO_2 thermal gate oxide. The NC films were treated with different cations by dipping into 50 mM solutions of corresponding metal nitrates in methanol, followed by rinsing the films with neat solvent. The films were then annealed at 200 °C, followed by patterning source and drain Al electrodes by using a shadow mask (channel length 150 μm, width 1500 μm). As-deposited NC solids contained residual solvent molecules and nitrate ions observed as additional peaks in the XPS spectra at 399.6 eV (N 1s peak with the binding energy typical for FA) and at 406.8 eV (N 1s peak with the binding energy typical for nitrate ions) shown in Figure S8. The annealing step allowed evaporation of residual solvent molecules coordinated to NC surface and further increased electronic coupling between CdSe NCs, evidenced by additional broadening of the excitonic peaks (Figure 3A). At the same time, this annealing temperature was insufficient to sinter CdSe NCs, as seen by the blue shift of the absorption onset with respect to the bulk CdSe band gap (1.74 eV or 713 nm) and by powder X-ray diffraction pattern typical for 4.2 nm CdSe NCs (Figure S9).

All FET devices assembled from CdSe/S^{2-} NCs supported n-type transport which agreed with the previous studies.[6] When positive bias is applied to the gate terminal ($V_G > 0$), electrons are injected into the FET channel and provide additional doping to the NC film resulting in a dramatic increase of the channel current. Figure 4A,B shows the output characteristics (i.e., drain current I_{DS} as a function of source−drain voltage V_{DS} at different gate voltages V_G) for FETs made of CdSe/S^{2-} NCs with K^+ counterions and for the same films cross-linked with Cd^{2+} ions. The cross-linking of NCs with Cd^{2+} resulted in ~100-fold increase in I_{DS} values for comparable V_G. Large difference in the channel currents can be seen in the transfer curves (I_{DS} vs V_G at fixed V_{DS}) for both devices (Figure 4C). The ratio of drain currents at V_G = 30 V and V_G = −10 V was $I_{ON}/I_{OFF} \approx 10^4$ and 10^7 for the pristine and Cd^{2+}-treated CdSe/S^{2-} NC films, respectively (Figure S10). The slope of the I_{DS} vs V_G curves at V_{DS} = 3 V was used to calculate the electron mobility corresponding to the linear regime of FET operation (μ_{lin}).[3,25] It revealed a large increase in the electron mobility, from μ_{lin} = 0.01 $cm^2 V^{-1} s^{-1}$ for NC films with K^+ counterions to 1.3 $cm^2 V^{-1} s^{-1}$ for those bridged with Cd^{2+}. Reproducible enhancement of the electron mobility were observed for the films treated with other cations like Mn^{2+}, Zn^{2+}, and In^{3+}, establishing a generic trend for NCs linked with different cations (Figures 4G and S11). The large increase of carrier mobility after Cd^{2+} or Zn^{2+} treatment was caused by the linking adjacent NCs, which also explains the broadening and red-shift in UV−vis absorption spectra (Figure 3A). The impact of different metal ions on mobility enhancement probably depends on multiple factors, for example, the chemical affinity of the metal to NC surface, extent of passivation of surface trap states by the metal ions, and the electronic structure of the NC/S^{2-}−M^{n+}−S^{2-}/NC interface. Our earlier studies revealed that CdSe/ZnS and CdSe/CdS core/shell NCs showed lower electron mobility compared to CdSe NCs; particularly, CdSe/

dx.doi.org/10.1021/ja301285x | J. Am. Chem. Soc. 2012, 134, 13604−13615

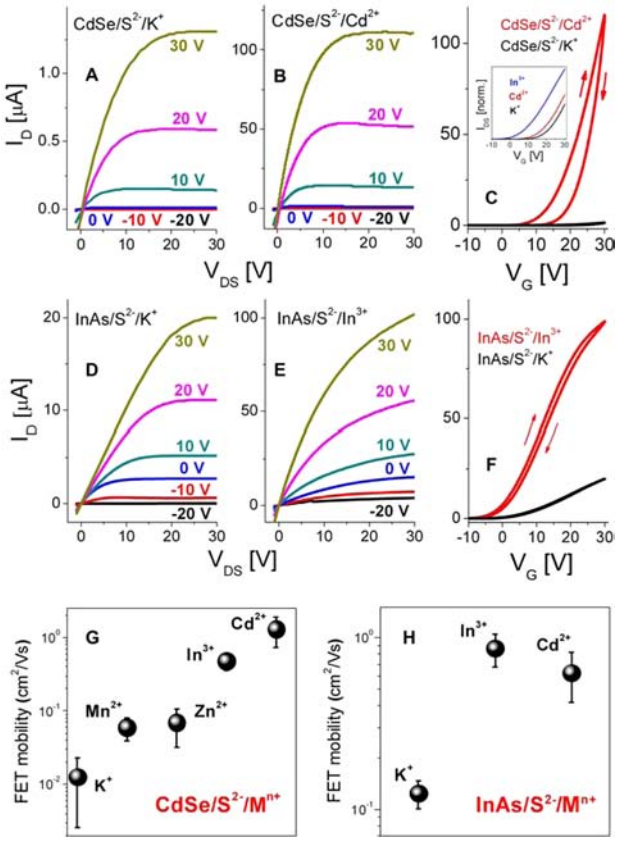

Figure 4. Effect of metal ions on the electron mobility in all-inorganic NC solids. Output characteristics, I_D vs V_{DS} as a function of gate voltage V_G for the field-effect devices (FETs) using films of (A) 4.2 nm CdSe NCs capped with K_2S ($CdSe/S^{2-}/K^+$) and (B) $CdSe/S^{2-}$ NCs treated with Cd^{2+} ions ($CdSe/S^{2-}/Cd^{2+}$). (C) Transfer characteristics, I_D vs V_G at V_{DS} = 3 V for FET devices using $CdSe/S^{2-}/K^+$ and $CdSe/S^{2-}/Cd^{2+}$ NC solids. The inset shows the turn-on gate voltage (V_{th}) for $CdSe/S^{2-}$ NCs treated with different cations. (D,E) Output characteristic and (F) transfer characteristics for FETs made of K_2S-capped 4.5 nm InAs NCs before ($InAs/S^{2-}/K^+$) and after ($InAs/S^{2-}/In^{3+}$) treatment with In^{3+} ions. (G,H) Effect of different metal ions on the field-effect electron mobility in $CdSe/S^{2-}$ $InAs/S^{2-}$ NC films, respectively.

ZnS NCs exhibited rather poor electron mobility ($\sim 10^{-5}$ cm^2 V^{-1} s^{-1}) because of additional tunneling barriers imposed by the shell material.[6] In a similar manner, we expect that μ_{lin} in metal-bridged all-inorganic NC solids should correlate with the alignment of the NC $1S_e$ state and the LUMO of the $S-M^{n+}-S$ bridge. Indeed, the comparison of the conduction band energies (E_{CB}) for corresponding metal sulfides $E_{CB}(K_2S) > E_{CB}(MnS) > E_{CB}(ZnS) > E_{CB}(In_2S_3) > E_{CB}(CdS)$[41] correlated with the mobility trend in Figure 4G. At the same time, such a simplistic approach should be used with great caution since it does not take into account the differences in the binding affinity for different metal ions discussed in section 3.1, modification of surface trap states by metal ion binding, and possible effects of the local coordination environment on the LUMO energy of the interparticle bridges.

The effect of metal ion linking on electron mobility was also observed for III–V InAs NCs (Figures 4D–F,H and S12), again showing a clear enhancement of the electron mobility after bridging $InAs/S^{2-}$ NCs with metal ions. $InAs/S^{2-}/In^{3+}$ NCs exhibit slightly higher electron mobility compared to $InAs/S^{2-}/Cd^{2+}$ NCs, a trend that cannot be rationalized simply on the basis of consideration of E_{CB} at the $S-M^{n+}-S$ interface. The binding affinity, local coordination environment and disorder at the $S-M^{n+}-S$ interface may contribute to the electron mobility in InAs NC solids. The cation linking was also effective for CdSe NCs capped with Li_2S and K_2Se (Figure S13). The use of metal linkers in combination with rapid thermal annealing allowed us to achieve rather high electron mobilities in NC solids, up to μ_{lin} = 7 cm^2 V^{-1} s^{-1} (Figure S14). En route, such high FET mobility was achieved using NCs processed from an environmentally benign FA solvent.

Carrier mobility reflects the connectivity between neighboring NCs whereas the FET threshold gate voltage (V_{th}) reflects the initial concentration of charge carriers in the channel (i.e., the doping level). Generally, lower V_{th} implies higher doping of the NC solid.[42] We compared the effect of different cations on V_{th} and observed that $CdSe/S^{2-}$ NCs bridged with In^{3+} ions showed a lower V_{th} than those bridged with Cd^{2+} ions (inset to Figure 4C). In turn, the NCs with K^+ counterions showed even higher V_{th} values. We can explain this trend by drawing a comparison between inter-NC bridges (Figure 3B) and substitutional dopants in conventional semiconductors. Indeed, when a monovalent cation (e.g., K^+) occupies a divalent (Cd^{2+}) lattice site, it typically creates an acceptor level and behaves as a p-type dopant. On the other hand, In^{3+} integrated in the CdSe lattice behaves as an n-type dopant. A similar trend in V_{th} was observed for InAs NCs bridged with K^+, Cd^{2+}, and In^{3+} ions. We therefore concluded that metal ions bridging all-inorganic NCs interact strongly with NCs and can control not only the carrier mobility but also the concentration of charge carriers in the NC solids.

3.4. Surface Metal Ions Can Determine the Type of Majority Carriers in All-Inorganic Nanocrystal Solids. To further explore the ability of inter-NC metal bridges to control doping in NC solids, we studied charge transport in CdTe NC arrays. CdTe is a II–VI semiconductor that can support both p-type and n-type transport, depending on the native defects and impurity doping.[43] K_2Te-capped colloidal CdTe NCs were prepared following standard organic-to-inorganic ligand exchange.[6] The films of as-synthesized $CdTe/Te^{2-}/K^+$ NCs formed a p-type transistor channel (Figures 5A,E, and S15). Depending on the FET geometry and electrode material, measured hole mobility was in the range 10^{-6}–10^{-4} cm^2 V^{-1} s^{-1}. p-Type mobility was also dominant when the films of K_2Te-capped CdTe NCs were treated with Cd^{2+} ions (Figure S16). According to the previous studies, electron-accepting (p-type) states in CdTe NCs arise from under-coordinated surface Te^{2-} sites,[44] while Cd^{2+} vacancies also give rise to the p-type doping in bulk CdTe.[45] On the other hand, In^{3+} doping in bulk CdTe is known to generate shallow donor states responsible for n-type conductivity.[43] When we treated $CdTe/Te^{2-}$ NCs with In^{3+} ions, the obtained NC solids exhibited ambipolar transport (Figure 5B,C,F,G), with significantly enhanced n-type transport compared to the NC films treated with Cd^{2+}. To further enhance n-type transport in the CdTe NC solids, we increased the concentration of In^{3+} ions at the NC surface by using $In_2Se_4^{2-}$ metal chalcogenide complexes instead of electron-accepting Te^{2-} ligands. $CdTe/In_2Se_4^{2-}$ NC solids showed strong n-type conductivity with electron mobility approaching 0.1 cm^2 V^{-1} s^{-1} (Figures 5C and S17). To the best of our knowledge, these charge carrier mobilities are the highest reported for CdTe NC solids.[44]

These results show that metal ions can efficiently control the type of conductivity in arrays of all-inorganic semiconductor

dx.doi.org/10.1021/ja301285x | J. Am. Chem. Soc. 2012, 134, 13604–13615

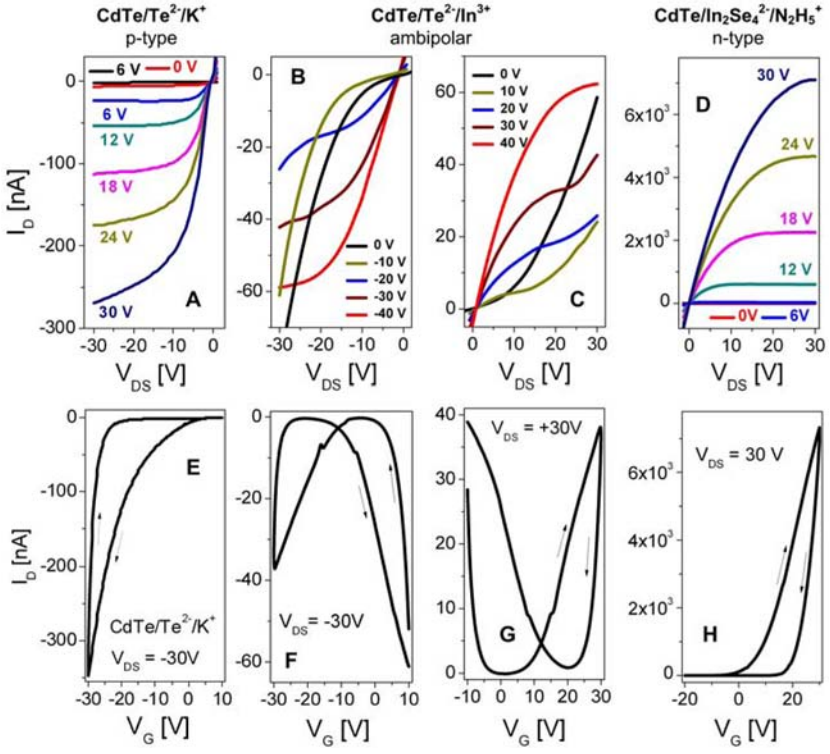

Figure 5. Output characteristics, I_D vs V_{DS} as a function of gate voltage V_G for FET devices using (A) K_2Te-capped CdSe NC films ($CdTe/Te^{2-}/K^+$) and (B,C) the same films treated with In^{3+} ions ($CdTe/Te^{2-}/In^{3+}$). (D) Output characteristics for an n-type FET using CdTe NCs capped with $In_2Se_4^{2-}$ ions ($CdTe/In_2Se_4^{2-}$). (E–H) Transfer characteristics, I_D vs V_G in the saturation limit for FET devices made of (E) $CdTe/Te^{2-}/K^+$ NCs, (F,G) $CdTe/Te^{2-}/In^{3+}$ NCs, and (H) $CdTe/In_2Se_4^{2-}$ NCs. The data shown in panels A–C and E–G were obtained using bottom gate/bottom source–drain FET device geometry (Ti/Au source and drain electrodes, channel length = 5 μm and width = 7800 μm). Data in panels D and H were obtained using bottom gate/top source–drain FET geometry (Al electrodes, channel length = 150 μm and width = 1500 μm). Additional data with different device geometries are shown in Figures S15 and S17.

NCs. This effect is conceptually similar to the remote doping, where ionized impurities are not directly integrated into semiconductor lattice but located in a close proximity that allows efficient charge transfer from dopant to semiconductor.[46] Taking into account difficulties with direct non-isovalent doping of semiconductor NCs,[47] the use of non-isovalent bridges for all-inorganic NCs provides a viable alternative for design of doped NC solids. Future studies will be necessary to fully understand and optimize doping in all-inorganic NC solids.

3.5. Magnetic Properties of CdSe and InAs NCs Linked with Mn^{2+} Ions. In addition to tuning the electronic properties of NC solids, cationic linkers can be used to introduce new functionalities to all-inorganic NC solids. As an example, Mn^{2+} ions can be used to introduce magnetism to non-magnetic $CdSe/S^{2-}$ NCs. For this study, a colloidal solution of K_2S-capped CdSe NCs in FA was precipitated by adding Mn^{2+} ions.[25] The elemental analysis showed a complete displacement of K^+ with Mn^{2+}, leading to a Mn-to-Cd ratio of 1:6.7, corresponding to about 13 molar % Mn^{2+} with respect to Cd^{2+}. This value sets an upper limit, corresponding to about 0.3 monolayer coverage of the 4.2 nm CdSe NC surface with Mn^{2+} ions. A lower doping level (e.g., 0.5% Mn) can be easily achieved by using mixtures of Mn^{2+} and Cd^{2+} ions (1:5.7 molar ratio) for NC linkage. In all cases, the XRD patterns of CdSe NCs remained identical before and after the Mn^{2+} treatment, suggesting binding of Mn^{2+} to the NC surface without forming any impurity phases (Figure S18).

Bulk CdSe is diamagnetic, with temperature-independent magnetic susceptibility $\chi_m \approx -3.3 \times 10^{-7}$ cm^3/g.[48] There are previous reports on ligand-induced paramagnetism of CdSe NCs,[49] but we observed a diamagnetic response of 4.2 nm CdSe NCs capped with K_2S ($\chi_m \approx -7 \times 10^{-7}$ cm^3/g). Figure 6 shows magnetization (M) vs magnetic field strength (H) plots for $CdSe/S^{2-}$ NCs before and after exchange of K^+ ions for

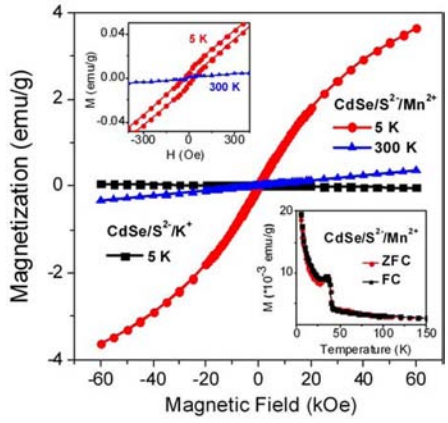

Figure 6. Magnetization (M) vs field (H) plots for K_2S-capped CdSe NCs, before ($CdSe/S^{2-}/K^+$) and after ($CdSe/S^{2-}/Mn^{2+}$) treatment with Mn^{2+} ions. Upper left inset shows M–H data for $CdSe/S^{2-}/Mn^{2+}$ in the low-field region. Bottom right inset shows ZFC and FC curves measured at 100 Oe for $CdSe/S^{2-}/Mn^{2+}$ NCs.

dx.doi.org/10.1021/ja301285x | J. Am. Chem. Soc. 2012, 134, 13604–13615

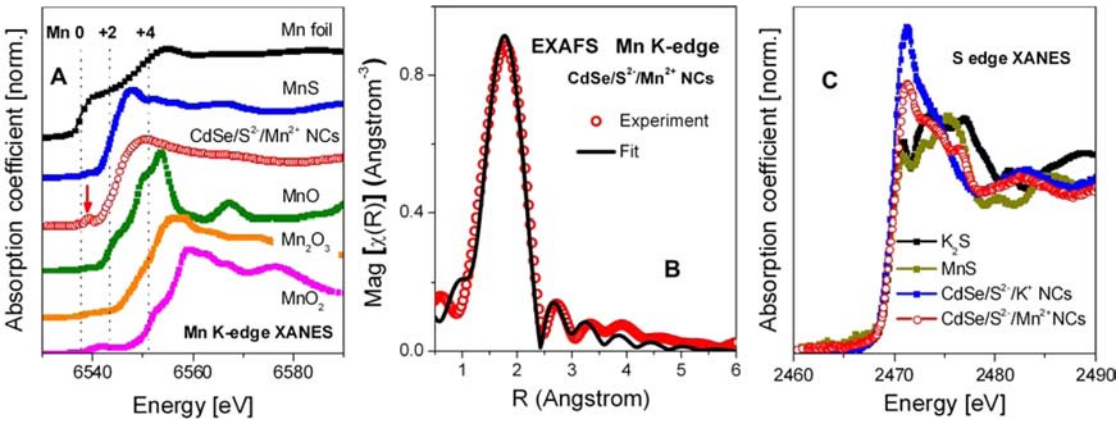

Figure 7. (A) Comparison of Mn K-edge XANES spectra for Mn^{2+}-treated, K_2S-capped CdSe NCs ($CdSe/S^{2-}/Mn^{2+}$) with standard compounds containing Mn in different oxidation states. (B) Magnitude of the Fourier transformed Mn K-edge EXAFS data and the fit for $CdSe/S^{2-}/Mn^{2+}$ NCs. See text and Supporting Information for details. (C) Comparison of the S-edge XANES spectra for $CdSe/S^{2-}/K^+$ and $CdSe/S^{2-}/Mn^{2+}$ NCs with XANES spectra of K_2S and MnS used as standards.

Mn^{2+}. Mn^{2+} ions imparted positive magnetic susceptibility combined with a hysteretic magnetization with a small coercivity ~40 Oe at 5 K, which vanished at 300 K (Figure 6, top left inset). At room temperature, CdSe NC solids bridged with Mn^{2+} ions showed field-independent paramagnetic response with $\chi_m \approx 5.9 \times 10^{-6}$ cm^3/g. Similar behavior was observed for 4.5 nm $InAs/S^{2-}$ NCs linked with Mn^{2+} ions. In the case of $InAs/S^{2-}/Mn^{2+}$ NCs, high-temperature paramagnetic behavior can be described by the Curie–Weiss law $1/\chi = (T - \theta)/C$, where C is the Curie constant, T is temperature, and θ is the Curie temperature (Figure S19). The negative θ value −22 K is indicative of the antiferromagnetic (AFM) exchange interaction between Mn^{2+} ions. Similar AFM coupling was observed for Mn^{2+} doped into the lattice of various semiconductors both in bulk and in NCs.[50−53] The magnetic susceptibility of $CdSe/S^{2-}/Mn^{2+}$ NCs showed more complex behavior, with a significant contribution from temperature-independent paramagnetism (Figure S19). Very recently, Zheng and Strouse observed similar behavior for Mn-doped CdSe NCs and ascribed it to the Pauli paramagnetism arising from the interactions of Mn^{2+} dopants with intrinsic carriers associated with NC surface states.[54]

The bottom right inset in Figure 6 shows ZFC and FC (100 Oe) magnetization data for $CdSe/S^{2-}/Mn^{2+}$ NCs, revealing a magnetic transition with the blocking temperature about 34 K that can be similar to the formation of a ferrimagnetic phase in CdSe NCs doped with Mn^{2+} ions.[52,54] When combined with good electronic properties provided by electronically transpired inorganic ligands, it should open up interesting opportunities for spintronic applications of all-inorganic NC solids. For example, charging NCs by applying gate voltage could induce ferromagnetic ordering of the magnetic moments of Mn^{2+} d-electrons.[55] We may also expect fundamental differences between CdSe NCs substitutionally doped with Mn^{2+} and those bridged with Mn^{2+} ions. This comes from the different local environment for Mn^{2+} ions, possible differences in the oxidation state, and the interaction of metal bridges with the NC core. The local environment is of great importance for all inter-NC metal ion bridges. We therefore applied EPR, XANES, and EXAFS techniques to better understand the bonding and local structure of Mn^{2+} ions in our system.

3.6. Probing Local Environment of Mn^{2+} Ions Linking CdSe NCs by EPR, XANES, and EXAFS Spectroscopy. Mn^{2+} has five unpaired electrons, and its local environment can be probed by EPR spectroscopy. Figure S20 shows the EPR spectrum measured at 4.6 K for $CdSe/S^{2-}$ NCs cross-linked with Mn^{2+} ions. This spectrum can be deconvoluted into two overlapping components: (i) a broad signal arising from the exchange coupled Mn^{2+} ions, and (ii) a characteristic sextet arising from the hyperfine interaction of the electron spin with ^{55}Mn nucleus ($I = 5/2$) of isolated Mn^{2+} ions. The measured Landé g-factor of 2.002 is closer to that for Mn^{2+}:CdS than to the g-factor for Mn^{2+}:CdSe (2.004),[56] which suggests that the local coordination of Mn^{2+} ions can be sulfur-rich, in accord with the bonding shown in Figure 1A. At the same time, the hyperfine coupling constant $A_{iso} = 86 \times 10^{-4}$ cm^{-1} (9.2 mT) is significantly larger than that for tetrahedrally coordinated Mn^{2+} in bulk CdS and CdSe lattices (65×10^{-4} and 62×10^{-4} cm^{-1}, respectively).[52,54] The large value of hyperfine splitting is characteristic of Mn^{2+} ions residing at the NC surface.[57,58] For example, $A_{iso} = 85 \times 10^{-4}$ cm^{-1} was reported for Mn^{2+} ions localized at the surface of CdSe NCs,[57] but for Mn^{2+} doped into a II–VI semiconductor NC lattice, $A_{iso} < 70 \times 10^{-4}$ cm^{-1}.[59−61] The 4.5 nm InAs NCs capped with S^{2-} ligands and bridged with Mn^{2+} ions revealed similar g-factor and A_{iso} (Figure S22), suggesting that, in both $CdSe/S^{2-}/Mn^{2+}$ and $InAs/S^{2-}/Mn^{2+}$ NCs, the manganese ions are bound to the surface through the same ligand and do not penetrate into the NC lattice.

X-ray absorption near-edge structure (XANES) spectroscopy provided additional information about the oxidation of surface Mn and S atoms at the surface of all-inorganic NCs, while extended X-ray absorption fine structure (EXAFS) spectroscopy was employed to probe the local environment around Mn ions on the surface of $CdSe/S^{2-}$ NCs.[25] The degree of edge shift, obtained via comparison of Mn K-edge XANES for the Mn^{2+}-treated NC sample ($CdSe/S^{2-}/Mn^{2+}$) with different Mn standards (Figure 7A), is indicative of +2 oxidation state, similar to that in bulk MnS. At the same time, differences in the shapes of the XANES spectra for $CdSe/S^{2-}/Mn^{2+}$ NCs and MnS indicate that the local structure around Mn^{2+} in the NC sample is unique. Particularly, in the NC sample, the Mn K-edge XANES revealed a strong pre-edge absorption peak (highlighted with the arrow in Figures 7A and S23) that corresponds to the dipole-forbidden 1s→3d transition. The intensity of this transition allows probing the local environment for Mn^{2+}. Thus, the pre-edge peak is absent or very weak for

dx.doi.org/10.1021/ja301285x | J. Am. Chem. Soc. 2012, 134, 13604−13615

centrosymmetric metal sites with O_h symmetry typical for MnS and MnO phases with rock salt structure.[62,63] The observation of a strong 1s→3d transition suggests non-centrosymmetric, e.g., tetrahedral (T_d), coordination of Mn^{2+} ions. The relative intensities of the pre-edge (1s→3d) and edge (1s→4p) transition in CdSe/S^{2-}/Mn^{2+} NCs were similar to those reported for isoelectronic Fe^{3+} sites with T_d symmetry in Fe-doped Na_2SiO_3 glass[64] and for tetrahedral Mn^{2+} doped into ZnO wurtzite lattice.[65]

Further information on the coordination environment for Mn^{2+} sites in CdSe/S^{2-}/Mn^{2+} NCs can be obtained from the analysis of EXAFS spectra. Figure 7B shows the magnitude of the Fourier transform (FT) of Mn K-edge EXAFS data for CdSe/S^{2-}/Mn^{2+} NC sample and the corresponding fit using the Mn−S path generated from MnS with zinc blende structure using FEFF6.[27] The fitting procedure together with the real part of the FT data and the best-fit parameters are shown in the Supporting Information (Figure S24 and Table S1). This analysis suggests that Mn atoms are bonded to S atoms with average Mn−S coordination number (CN) = 3.1 and bond length = 2.37 Å. The obtained CN is slightly smaller than the typical tetrahedral (CN = 4, wurtzite and zinc blend) and octahedral (CN = 6, rock salt) coordination. At the same time, the obtained bond length is close to the theoretical bond length of the Mn−S path in the MnS with wurtzite and zinc blende phases (~2.41 Å) but significantly shorter than the bond length for the Mn−S path in MnS with rock salt structure (2.62 Å). This reduced Mn−S CN and bond length for CdSe/S^{2-}/Mn^{2+} NC sample suggest Mn^{2+} binding exclusively to the NCs surface, which was also demonstrated independently by XRD and EPR studies. The combination of intense pre-edge peak observed in XANES spectra with the bond length and CN obtained from EXAFS fits rules out the possibility of the formation of MnS phase and supports a tetrahedral-like coordination environment for Mn^{2+} sites at the NC surface.

The S-edge XANES data of K_2S-capped CdSe NCs before (CdSe/S^{2-}/K^+) and after (CdSe/S^{2-}/Mn^{2+}) Mn^{2+} treatment along with several sulfur standards are shown in Figures 7C and S25. The difference of XANES spectra between K_2S and CdSe/S^{2-}/K^+ NCs agree with the preconceived notion that S^{2-} binds covalently to the Cd^{2+} sites at the surface of CdSe NCs. More importantly, the XANES data for CdSe/S^{2-}/Mn^{2+} NC samples can be reasonably well fitted as a superposition of S-edge XANES spectra for CdSe/S^{2-}/K^+ NCs and MnS. A linear combination fit shows that the XANES spectrum for CdSe/S^{2-}/Mn^{2+} NCs can be modeled as 55% contribution from CdSe/S^{2-}/K^+ NC and 45% from MnS, once again suggesting the formation of Cd−S−Mn bonds on the NC surface (Figure S26 and Table S2).

When combined, EPR, XANES, and EXAFS studies suggest that Mn^{2+} ions bind to the surface of CdSe/S^{2-} NCs without changes of their oxidation state. The Mn^{2+} primarily bind to the electron-rich S^{2-} ligands at the NC surface with tetrahedral-like coordination environment, average CN = 3.1, and Mn−S bond length = 2.37 Å. At the same time, S^{2-} ligands bind simultaneously to Cd^{2+} and Mn^{2+} ions, behaving as bridges for electronic coupling of paramagnetic Mn^{2+} ions to CdSe NCs.

We want to emphasize that the local coordination environment of bridging ions may vary across the NC solid. Such disorder is an inherent property of randomly packed NC solids, as evident from the high-resolution TEM (Figure S7). The average CN = 3.1 extracted from EXAFS fits can be explained by the presence of different coordination sites, where some Mn^{2+} ions have CN = 2, while others have CN = 4 or even 6. The presence of a strong pre-edge feature in the Mn edge at 6539 eV suggests that a considerable fraction of Mn^{2+} ions preserves tetrahedral environment (CN = 4) without an inversion symmetry. We may also expect the possibility of linear S−Mn−S bridges where Mn^{2+} is octahedrally coordinated with two S^{2-} ligands and four solvent molecules (D_{4h} point symmetry at the metal center).

3.7. Pt^{2+} Bridges Can Be Used To Enhance the Electrocatalytic Properties of All-Inorganic Nanocrystal Solids. The ability to tailor the optical, magnetic, and charge transport properties of NCs by interacting them with a suitable metal ion motivated us to bind catalytically active ions to the NC surface that combine tunable electronic structure with high surface-to-volume ratio. The NC surface can be modified with oxidation or reduction catalysts, such as such transition metal nanoparticles,[66] MoS_3,[67] or enzymes.[68] Here we show that transition metal ions bound to the surface of all-inorganic NCs can be used to mediate redox processes at the NC surface. To demonstrate this effect, we compared the electrochemical properties of CdSe/S^{2-} NCs with different counterions, K^+ and Pt^{2+}, in a model electrochemical reaction of proton reduction and hydrogen evolution in acetonitrile and aqueous media (Figure 8A). The first set of electrochemical measurements was

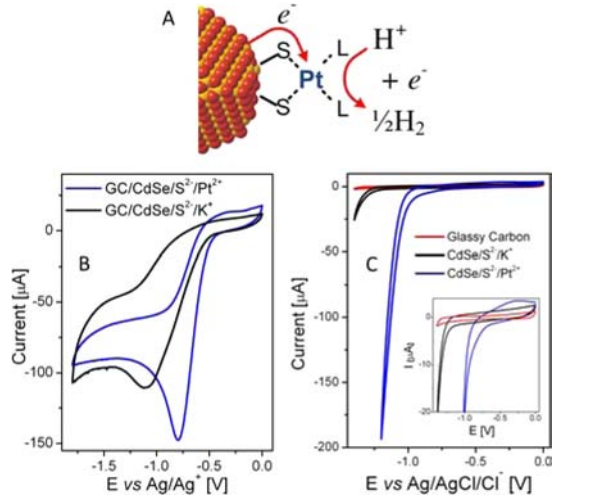

Figure 8. (A) Schematics of CdSe/S^{2-} NC surface with coordinated Pt^{2+} ions, showing that electrons supplied by NC can drive proton reduction. (B) Cyclic voltammograms measured for CdSe/S^{2-}/K^+ and CdSe/S^{2-}/Pt^{2+} NC films in anhydrous acetonitrile in the presence of 0.01 M [H(DMF)]OTf as a proton source and 0.1 M TBAP as an electrolyte. (C) Cyclic voltammograms measured for CdSe/S^{2-}/K^+ and CdSe/S^{2-}/Pt^{2+} NC films in aqueous solution buffered at pH 6.5 with a phosphate buffer. The inset shows onsets of hydrogen reduction processes for different electrodes.

performed in anhydrous acetonitrile inside a N_2-filled glovebox. Protonated DMF triflate [H(DMF)]OTf, behaving as a weak acid with pK_a = 6.1 in acetonitrile,[69] was used as a proton source, and TBAP was used as an electrolyte. The CdSe/S^{2-}/K^+ NC films were deposited on either ITO-covered glass or GC electrodes from FA solutions. A red-orange solution of $K_2[PtCl_4]$ was prepared in FA at 80 °C as a precursor for Pt^{2+}, following Kanatzidis et al.[70] As-deposited NC films showed the first absorption peak near 590 nm. Treatment of CdSe/S^{2-}/K^+ NC films with 0.1 M FA solution of $K_2[PtCl_4]$

dx.doi.org/10.1021/ja301285x | J. Am. Chem. Soc. 2012, 134, 13604−13615

for 30 min resulted in a 5 nm red-shift of the first absorption peak (Figure S28), indicating binding of Pt^{2+} to the NC surface, which probably enhanced the electronic coupling between NCs analogous to the data shown in Figure 3A. In control experiments we confirmed that neither the shape of the absorption spectrum nor the position of the first excitonic peak changed after five cycles of the electrode potential between −1.7 and 0 V vs Ag/Ag^+ reference electrode at 100 mV/s ($E_{Ag^+/Ag}$ = −0.125 V relative to Cp_2Fe^+/Cp_2Fe couple, as shown in Figure S27), indicating that CdSe NCs stayed intact over the course of electrochemical studies (Figure S28).

Cyclic voltammetry for $CdSe/S^{2-}/K^+$ and $CdSe/S^{2-}/Pt^{2+}$ NC films on GC electrode in the presence of 0.01 M [H(DMF)]OTf showed diffusion-limited proton reduction. The wave for $H(DMF)^+$ reduction on GC electrode was observed with a half-wave potential of −0.778 V vs Ag/Ag^+ reference electrode (Figure S29). It corresponds to an overpotential of ∼403 mV, as determined using the method described in ref 71. Deposition of the $CdSe/S^{2-}/K^+$ NC film on a GC surface increased the overpotential to ∼410 mV (Figure 8B, black curve). The exchange of K^+ ions with Pt^{2+} resulted in a significantly lower overpotential of ∼273 mV (Figure 8B, blue curve), in agreement with increased catalytic activity of the NC surface.

To study the electrocatalytic performance of all-inorganic NCs in aqueous media, we carried out similar measurements in aqueous solutions buffered at pH 6.50 with a phosphate buffer. At this pH, the Nernst equation gives $E(H_2/2H^+)$ = −0.38 V relative to the SHE or −0.58 V relative to the saturated $Ag/AgCl/Cl^-$ reference electrode used in this work. However, no hydrogen reduction was observed up to −1.4 V on GC because of low exchange currents for this reaction leading to high overpotentials.[71] Deposition of a 4.2 nm $CdSe/S^{2-}/K^+$ NC film on the GC electrode resulted in a minor improvement of catalytic activity (Figure 8C, black curve). After replacing the K^+ ions with Pt^{2+} by exposing the NC film to 0.1 M FA solution of $K_2[PtCl_4]$ for 30 min followed by careful rinsing with acetonitrile, we observed a strong enhancement of the faradaic current, with the current onset shifted to −0.736 V vs $Ag/AgCl/Cl^-$ (or ∼ −0.539 V vs SHE), as shown in Figure 8C. Tafel analysis revealed ∼50-fold enhancement of the exchange current, from ∼6 nA/cm^2 to 0.3 μA/cm^2, when K^+ ions were replaced with Pt^{2+}.[25] This improvement is not counterintuitive, since Pt is a well-known catalyst for hydrogen evolution reactions. At the same time, we want to emphasize that such significant improvement of the exchange current was observed only for NCs capped with S^{2-} ligands. In the control experiments, we exposed a freshly polished GC electrode or a film of CdSe NCs capped with TDPA to 0.1 M FA solution of $K_2[PtCl_4]$ and measured the effect of such treatment on electrochemical properties. In both cases, we observed only minor changes in cathodic current before and after treatment with $K_2[PtCl_4]$ (Figure S30). These results can be explained by inefficient adsorption of Pt^{2+} on GC and the TDPA-capped surface of CdSe NCs. In contrast, the exchange of K^+ ions with Pt^{2+} in $CdSe/S^{2-}/K^+$ NC solids occurred very efficiently at room temperature because of the accessibility of the NC surface and the presence of negatively charged S^{2-} groups exhibiting high chemical affinity to Pt(II) species. This study also demonstrates that charge carriers in all-inorganic semiconductor NCs can efficiently interact with redox catalysts at the NC surface. This proof-of-principle observation opens up multiple opportunities for rational design of electro- and photocatalytic systems where quantum-confined semiconductors supply non-equilibrium charge carriers for catalytic transformations.

4. CONCLUSIONS

In summary, we show that metal ions can interact with the surface of all-inorganic semiconductor NCs to allow engineering of the NC properties both in solution and in close-packed NC solids. For example, Cd^{2+}, Ca^{2+}, and Zn^{2+} can efficiently bind to S^{2-}-capped CdSe or CdSe/ZnS core−shell NCs in dilute solutions, inversing the surface charge from negative to positive and significantly increasing the luminescence efficiency. In an array of K_2S-capped CdSe NCs, the treatment with suitable metal ions allows replacing weakly bound K^+ ions and linking adjacent NCs. The formation of inter-NC bridges enhances charge carrier mobility by 2 orders of magnitude, leading to an electron mobility of 1.3 cm^2 V^{-1} s^{-1} achieved via a benign hydrazine-free device processing. The metal ion linkers also allow tailoring the doping in the NC solids, switching CdTe NC FETs from p-type to ambipolar to n-type. EPR and EXAFS spectroscopy carried out for CdSe NCs with S^{2-} ligands bridged by Mn^{2+} ions confirmed that Mn^{2+} bonded to the S^{2-}-capped CdSe NC via S−Mn−S bonds with bond length = 2.37 Å and average CN = 3.1. NCs with Mn^{2+} on the surface exhibit superparamagnetic behavior. Magnetization studies showed that bridging with Mn^{2+} ions can switch the magnetic properties of NC solids from dia- to paramagnetic at room temperature and to a magnetically ordered phase at low temperature. Finally, we demonstrated that bridging CdSe NCs with Pt^{2+} ions improves the electrocatalytic properties of all-inorganic NCs in the hydrogen evolution reaction, in both aqueous and acetonitrile media. These examples show the generality and versatility of our approach for tailoring physical and chemical properties of a broad class of NC-based materials.

■ ASSOCIATED CONTENT

Supporting Information

Additional experimental details, figures, and tables. This material is available free of charge via the Internet at http://pubs.acs.org.

■ AUTHOR INFORMATION

Corresponding Author

dvtalapin@uchicago.edu

Notes

The authors declare no competing financial interest.

■ ACKNOWLEDGMENTS

The authors thank D. Moravec and M. D. Hopkins for PL lifetime measurements; Elena V. Shevchenko for magnetic measurements; T. Wang and S. Sibener for XPS measurements; and W. Liu, J. Huang, and Evident Technologies Inc. for InAs NCs, CdS nanorods, and CdSe/ZnS core/shell NCs, respectively. S.C. acknowledges S. Heald, S. Kwon, V. Zyranov, T. Bolin, and C. U. Segre for help with the EXAFS/XANES measurements. The work on charge inversion, magnetic, and structural studies was supported by NSF CAREER under Award No. DMR-0847535; the work on charge transport in cation-bridged NC arrays was supported by the Office of Naval Research under Award No. N00014-10-1-0190, and the work on doping of CdTe NC solids was supported by the DOE SunShot program under Award No. DE-EE0005312. D.V.T.

also thanks the David and Lucile Packard Foundation for their generous support. This work used facilities supported by NSF MRSEC Program under Award No. DMR-0213745. ICP-OES elemental analysis was carried out at the Analytical Chemistry Laboratory at Argonne National Lab (ANL). MRCAT operations are supported by the Department of Energy and the MRCAT member institutions. The use of the Advanced Photon Source at ANL was supported by the U.S. Department of Energy, Office of Science, Office of Basic Energy Sciences, under Contract No. DE-AC02-06CH11357. The work at the Center for Nanoscale Materials (ANL) was supported by the U.S. Department of Energy under Contract No. DE-AC02-06CH11357.

REFERENCES

(1) Coe, S.; Woo, W. K.; Bawendi, M.; Bulovic, V. *Nature* **2002**, *420*, 800−803.
(2) Konstantatos, G.; Howard, I.; Fischer, A.; Hoogland, S.; Clifford, J.; Klem, E.; Levina, L.; Sargent, E. H. *Nature* **2006**, *442*, 180−183.
(3) Talapin, D. V.; Lee, J. S.; Kovalenko, M. V.; Shevchenko, E. V. *Chem. Rev.* **2010**, *110*, 389−458.
(4) Kovalenko, M. V.; Scheele, M.; Talapin, D. V. *Science* **2009**, *324*, 1417−1420.
(5) Lee, J. S.; Kovalenko, M. V.; Huang, J.; Chung, D. S.; Talapin, D. V. *Nat. Nanotechnol.* **2011**, *6*, 348−352.
(6) Nag, A.; Kovalenko, M. V.; Lee, J. S.; Liu, W. Y.; Spokoyny, B.; Talapin, D. V. *J. Am. Chem. Soc.* **2011**, *133*, 10612−10620.
(7) Fafarman, A. T.; Koh, W. K.; Diroll, B. T.; Kim, D. K.; Ko, D. K.; Oh, S. J.; Ye, X. C.; Doan-Nguyen, V.; Crump, M. R.; Reifsnyder, D. C.; Murray, C. B.; Kagan, C. R. *J. Am. Chem. Soc.* **2011**, *133*, 15753−15761.
(8) Tang, J.; Kemp, K. W.; Hoogland, S.; Jeong, K. S.; Liu, H.; Levina, L.; Furukawa, M.; Wang, X. H.; Debnath, R.; Cha, D. K.; Chou, K. W.; Fischer, A.; Amassian, A.; Asbury, J. B.; Sargent, E. H. *Nat. Mater.* **2011**, *10*, 765−771.
(9) Grosberg, A. Y.; Nguyen, T. T.; Shklovskii, B. I. *Rev. Mod. Phys.* **2002**, *74*, 329−345.
(10) dos Santos, A. P.; Levin, Y. *Phys. Rev. Lett.* **2011**, *106*, 4.
(11) Kovalenko, M. V.; Bodnarchuk, M. I.; Zaumseil, J.; Lee, J. S.; Talapin, D. V. *J. Am. Chem. Soc.* **2010**, *132*, 10085−10092.
(12) Kovalenko, M. V.; Bodnarchuk, M. I.; Talapin, D. V. *J. Am. Chem. Soc.* **2010**, *132*, 15124−15126.
(13) Son, D. H.; Hughes, S. M.; Yin, Y. D.; Alivisatos, A. P. *Science* **2004**, *306*, 1009−1012.
(14) Jain, P. K.; Amirav, L.; Aloni, S.; Alivisatos, A. P. *J. Am. Chem. Soc.* **2010**, *132*, 9997−9999.
(15) Fedorov, V. A.; Ganshin, V. A.; Korkishko, Y. N. *Phys. Status Solidi A-Appl. Res.* **1993**, *139*, 9−65.
(16) Dalpian, G. M.; Chelikowsky, J. R. *Phys. Rev. Lett.* **2006**, *96*, 226802.
(17) Chikan, V. *J. Phys. Chem. Lett.* **2011**, *2*, 2783−2789.
(18) Yang, Y. A.; Wu, H. M.; Williams, K. R.; Cao, Y. C. *Angew. Chem., Int. Ed.* **2005**, *44*, 6712−6715.
(19) Carbone, L.; Nobile, C.; De Giorgi, M.; Sala, F. D.; Morello, G.; Pompa, P.; Hytch, M.; Snoeck, E.; Fiore, A.; Franchini, I. R.; Nadasan, M.; Silvestre, A. F.; Chiodo, L.; Kudera, S.; Cingolani, R.; Krahne, R.; Manna, L. *Nano Lett.* **2007**, *7*, 2942−2950.
(20) Guzelian, A. A.; Banin, U.; Kadavanich, A. V.; Peng, X.; Alivisatos, A. P. *Appl. Phys. Lett.* **1996**, *69*, 1432−1434.
(21) Cao, Y. W.; Banin, U. *J. Am. Chem. Soc.* **2000**, *122*, 9692−9702.
(22) Talapin, D. V.; Nelson, J. H.; Shevchenko, E. V.; Aloni, S.; Sadtler, B.; Alivisatos, A. P. *Nano Lett.* **2007**, *7*, 2951−2959.
(23) Yu, W. W.; Qu, L. H.; Guo, W. Z.; Peng, X. G. *Chem. Mater.* **2003**, *15*, 2854−2860.
(24) Kovalenko, M. V.; Bodnarchuk, M. I.; Zaumseil, J.; Lee, J. S.; Talapin, D. V. *J. Am. Chem. Soc.* **2010**, *132*, 10085−10092.
(25) Additional details are provided as Supporting Information.
(26) Newville, M. *J. Synch. Radiat.* **2001**, *8*, 322−324.
(27) Rehr, J. J.; Albers, R. C. *Rev. Mod. Phys.* **2000**, *72*, 621−654.
(28) Ravel, B.; Newville, M. *J. Synch. Radiat.* **2005**, *12*, 537−541.
(29) Favier, I.; Dunach, E. *Tetrahedron Lett.* **2004**, *45*, 3393−3395.
(30) Nag, A.; Kovalenko, M. V.; Lee, J. S.; Liu, W. Y.; Spokoyny, B.; Talapin, D. V. *J. Am. Chem. Soc.* **2011**, *133*, 10612−10620.
(31) Henry, D. C. *Proc. R. Soc. London A* **1931**, *133*, 106−129.
(32) Hunter, R. J. *Foundations of Colloid Science*, 2nd ed.; Oxford University Press: New York, 2001.
(33) Calero, C.; Faraudo, J.; Bastos-González, D. *J. Am. Chem. Soc.* **2011**, *133*, 15025−15035.
(34) Shklovskii, B. I. *Phys. Rev. E* **1999**, *60*, 5802−5811.
(35) Messina, R.; Holm, C.; Kremer, K. *Phys. Rev. Lett.* **2000**, *85*, 872−875.
(36) Parr, R. G.; Pearson, R. G. *J. Am. Chem. Soc.* **1983**, *105*, 7512−7516.
(37) Verwey, E. J. W. *Chem. Rev.* **1935**, *16*, 363−415.
(38) Jasieniak, J.; Mulvaney, P. *J. Am. Chem. Soc.* **2007**, *129*, 2841−2848.
(39) Hines, M. A.; Guyot-Sionnest, P. *J. Phys. Chem.* **1996**, *100*, 468−471.
(40) Dabbousi, B. O.; RodriguezViejo, J.; Mikulec, F. V.; Heine, J. R.; Mattoussi, H.; Ober, R.; Jensen, K. F.; Bawendi, M. G. *J. Phys. Chem. B* **1997**, *101*, 9463−9475.
(41) Xu, Y.; Schoonen, M. A. A. *Am. Minerol.* **2000**, *85*, 543−556.
(42) Podzorov, V.; Menard, E.; Borissov, A.; Kiryukhin, V.; Rogers, J. A.; Gershenson, M. E. *Phys. Rev. Lett.* **2004**, *93*, 086602.
(43) Khattak, G. M.; Scott, C. G. *J. Phys. Condens. Matter* **1991**, *3*, 8619−8634.
(44) Geyer, S.; Porter, V. J.; Halpert, J. E.; Mentzel, T. S.; Kastner, M. A.; Bawendi, M. G. *Phys. Rev. B* **2010**, *82*, 155201.
(45) Bube,R. H. *Photoconductivity of Solids* ; Wiley: New York, 1960.
(46) Li, H. Y.; Wunnicke, O.; Borgstrom, M. T.; Immink, W. G. G.; van Weert, M. H. M.; Verheijen, M. A.; Bakkers, E. *Nano Lett.* **2007**, *7*, 1144−1148.
(47) Chan, T. L.; Zayak, A. T.; Dalpian, G. M.; Chelikowsky, J. R. *Phys. Rev. Lett.* **2009**, *102*, 025901.
(48) Landolt−Bornstein. *Numerical Data and Functional Relationships in Science and Technology*; Springer: Berlin/Heidelberg/New York, 1982; Vol. *17*: Semiconductors.
(49) Meulenberg, R. W.; Lee, J. R. I.; McCall, S. K.; Hanif, K. M.; Haskel, D.; Lang, J. C.; Terminello, L. J.; van Buuren, T. *J. Am. Chem. Soc.* **2009**, *131*, 6888−6889.
(50) Furdyna, J. K. J. *Appl. Phys.* **1988**, *64*, R29−R64.
(51) Feltin, N.; Levy, L.; Ingert, D.; Vincent, E.; Pileni, M. P. J. *Appl. Phys.* **2000**, *87*, 1415−1423.
(52) Magana, D.; Perera, S. C.; Harter, A. G.; Dalal, N. S.; Strouse, G. F. *J. Am. Chem. Soc.* **2006**, *128*, 2931−2939.
(53) Bryan, J. D.; Gamelin, D. R. *Prog. Inorg. Chem.* **2005**, *54*, 47−126.
(54) Zheng, W. W.; Strouse, G. F. *J. Am. Chem. Soc.* **2011**, *133*, 7482−7489.
(55) Ochsenbein, S. T.; Feng, Y.; Whitaker, K. M.; Badaeva, E.; Liu, W. K.; Li, X.; Gamelin, D. R. *Nat. Nanotechnol.* **2009**, *4*, 681−687.
(56) Beaulac, R.; Ochsenbein, S. T.; Gamelin, D. R. In *Nanocrystal Quantum Dots*, 2nd ed. Klimov, V. I., Ed.; CRC Press: Boca Raton, FL, 2010; pp 397−453.
(57) Mikulec, F. V.; Kuno, M.; Bennati, M.; Hall, D. A.; Griffin, R. G.; Bawendi, M. G. *J. Am. Chem. Soc.* **2000**, *122*, 2532−2540.
(58) Norris, D. J.; Yao, N.; Charnock, F. T.; Kennedy, T. A. *Nano Lett.* **2001**, *1*, 3−7.
(59) Jun, Y. W.; Jung, Y. Y.; Cheon, J. *J. Am. Chem. Soc.* **2002**, *124*, 615−619.
(60) Stowell, C. A.; Wiacek, R. J.; Saunders, A. E.; Korgel, B. A. *Nano Lett.* **2003**, *3*, 1441−1447.
(61) Nistor, S. V.; Stefan, M. *J. Phys. Condes. Matter* **2009**, *21*, 7.
(62) Farges, F. *Phys. Rev. B* **2005**, *71*, 155109.

(63) Droubay, T. C.; Keavney, D. J.; Kaspar, T. C.; Heald, S. M.; Wang, C. M.; Johnson, C. A.; Whitaker, K. M.; Gamelin, D. R.; Chambers, S. A. *Phys. Rev. B* **2009**, *79*, 155203.
(64) Lytle, F. W.; Greegor, R. B.; Panson, A. J. *Phys. Rev. B* **1988**, *37*, 1550−1562.
(65) Guglieri, C.; Céspedes, E.; Prieto, C.; Chaboy, J. *J. Phys. Condens. Matter* **2011**, *23*, 206006.
(66) Amirav, L.; Alivisatos, A. P. *J. Phys. Chem. Lett.* **2010**, *1*, 1051−1054.
(67) Tang, M. L.; Grauer, D. C.; Lassalle-Kaiser, B.; Yachandra, V. K.; Amirav, L.; Long, J. R.; Yano, J.; Alivisatos, A. P. *Angew. Chem., Int. Ed.* **2011**, *50*, 10203−10207.
(68) Curri, M. L.; Agostiano, A.; Leo, G.; Mallardi, A.; Cosma, P.; Della Monica, M. *Mater. Sci. Eng.: C* **2002**, *22*, 449−452.
(69) Helm, M. L.; Stewart, M. P.; Bullock, R. M.; DuBois, M. R.; DuBois, D. L. *Science* **2011**, *333*, 863−866.
(70) Trikalitis, P. N.; Rangan, K. K.; Kanatzidis, M. G. *J. Am. Chem. Soc.* **2002**, *124*, 2604−2613.
(71) Felton, G. A. N.; Glass, R. S.; Lichtenberger, D. L.; Evans, D. H. *Inorg. Chem.* **2006**, *45*, 9181−9184.